ELSEVIER

Polymer 42 (2001) 5803–5811

polymer

www.elsevier.nl/locate/polymer

Fatigue failure mechanisms of short glass-fiber reinforced nylon 66 based on nonlinear dynamic viscoelastic measurement

K. Noda[a], A. Takahara[b], T. Kajiyama[c,*]

[a]*Asahi Chemical Industry Co., Ltd, Kawasaki-ku, Kawasaki, Kanagawa 210-0863, Japan*
[b]*Institute for Fundamental Resarch of Organic Chemistry, Kyushu University, Higashi-ku, Fukuoka 812-8581, Japan*
[c]*Department of Applied Chemistry, Faculty of Engineering, Kyushu University, Higashi-ku, Fukuoka 812-8581, Japan*

Received 8 June 2000; received in revised form 1 December 2000; accepted 6 December 2000

Abstract

The fatigue behavior of short glass-fiber reinforced nylon 66 under stress controlled fatigue tests was studied on the basis of the nonlinear dynamic viscoelasticity measurements. In order to analyze the effect of nonlinear viscoelasticity on the fatigue behavior, quantitative measurements of nonlinear viscoelasticity have been carried out based on Fourier analysis. It was found that the nonlinear viscoelastic behavior that was closely related to the irreversible structural change appeared markedly during fatigue process. The failure models in fatigue process were proposed based on the cross-section morphology under optical microscopic observation before final failure of the specimens. The fatigue behavior could be classified into the two failure mechanisms, depending on whether the fatigue test was carried out below or above glass transition temperature of the matrix nylon 66. The fatigue process proceeded with the following steps:(1) the damage started with void formation at fiber ends; (2) the microcracks propagated around the fiber ends ($T \leqq T_g$) or the microcracks propagated being accompanied with debonding along the fiber sides and also, forming the crack walls($T > T_g$); (3) the cracks propagated between the fiber ends($T \leqq T_g$) in a brittle manner, or the crack walls dominantly remained being connected by bridges($T > T_g$) in a ductile manner; (4) the fast crack propagation occurred, after the crack reached to a critical size, and finally, the specimen failed.

Keywords: Fatigue failure mechanisms; Glass-fiber; Viscoelastic

1. Introduction

Recently polymer composite materials have been used in many structural applications. Metal parts have been replaced by thermoplastic composites reinforced with short glass-fiber because of cost and weight reductions in engineering applications. Thermoplastic composites reinforced with short glass fibers have high modulus and strength and they have been prepared by the injection molding process, which brings feasibility of design and integration of functions possible. Because the thermoplastic composites have been applied for the structural components as a replacement of metals with higher level of fatigue strength, it is necessary to improve the long term reliability of the short glass-fiber reinforced composites in order to enhance the lifetime of the composites. Especially, the fatigue characteristics are very important and the accurate prediction of fatigue lifetime is necessary for the design of structural component. Most of the present fatigue studies on the thermoplastic composites have been done based on classical testing method established for metals [1–3]. However, little attention has been paid to the viscoelasticity of the polymer composites that is a characteristic property of polymers. From such an engineering viewpoint, it is very important to clarify the fatigue mechanism and also to predict fatigue lifetime of polymer composites.

Even though the magnitude of loading cyclic stress is by far lower than that of tensile strength of the polymer materials, changes of structure and physical properties gradually proceed during cyclic loading and materials finally come to fracture. Though the tensile failure mechanism of composites has been studied more in detail [4], the fatigue has not been clarified yet. Lang et al. [1] and Horst and Spoormaker [5] discussed the differences between tensile fracture and fatigue fracture surfaces of short glass-fiber reinforced nylon specimens on the basis of SEM observation. In case of the tensile fracture, the fiber surface was covered with the polymer matrix, while in the case of the cyclic fatigue, the fiber surface was smooth without any adhered matrix. Hertzberg and Manson [2] reported that the fatigue damage started from debonding of the fibers that oriented

* Corresponding author. Tel.: +81-92-642-3558; fax: +81-92-651-5606.
E-mail address: kajiyama@cstj.kyushu-u.ac.jp (T. Kajiyama).

0032-3861/01/$ - see front matter
PII: S0032-3861(00)00897-1

perpendicular to the load axis. Though many investigations on the fatigue mechanism of thermoplastic polymer composites have been done, there is still no identical view.

On the other hand, the fatigue property of polymeric solids or polymer composites has been studied from a point of view of a viscoelastic change during cyclic fatigue [6–9]. Two types of brittle and ductile failures reported on the basis of continuous measurements of nonlinear dynamic viscoelasticity and a surface temperature during the fatigue process [6–9]. Also, the authors proposed the quantitative evaluation method on the nonlinear dynamic viscoelasticity, so-called the nonlinear viscoelastic parameter (NVP) analysis [10–15]. The magnitude of NVP can be calculated from the coefficients of the Fourier expanded series of the response signal and provides the information on the irreversible structural change during cyclic fatigue.

However, little study has been made to clarify the relationship between nonlinear dynamic viscoelasticity and irreversible structural change, such as crack initiation and crack growth during cyclic fatigue. If the irreversible structural change during cyclic fatigue can be directly evaluated on the basis of the nonlinear dynamic viscoelasticity, it is apparent that effective information on fatigue mechanism and prediction of fatigue lifetime can be obtained.

In this study, in order to clarify the fracture mechanism of short glass-fiber reinforced nylon 66 under stress control fatigue tests, the fatigue behavior was studied on the basis of nonlinear dynamic viscoelastic measurement, and the variation of fracture morphology during cyclic fatigue was observed. An aim of this study is to reveal the relationship between nonlinear viscoelasticity and fatigue mechanism and finally, to propose the model of fatigue fracture mechanism.

2. Experimental

2.1. Materials

The specimens for fatigue tests were injection-molded from nylon 66 containing 33 wt% glass-fiber reinforcement that treated with aminosilane coupling agent and sizing agent (Leona 14G33 provided by Asahi Chemical Industry Co. Ltd, Japan). Fig. 1 shows the shape and the dimensions of an ASTM-D1822 Type S tension-impact specimen. The diameter and the number average length of the glass fiber in the specimen were 10 and ca 300 μm, respectively. The glass-fibers in the minimum cross-section area of the specimen were almost oriented along the flow direction of the molding, that is, the longitudinal direction of the specimen. The moisture content of the specimen before and after the fatigue test was kept to be less than 0.2 wt%.

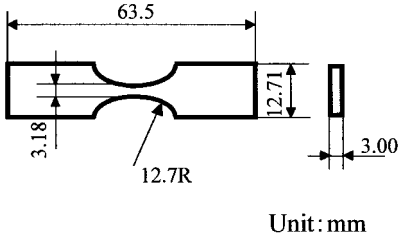

Fig. 1. Dimensions of ASTM-D1822 Type S tension-impact specimen.

2.2. Fatigue test

Fig. 2 shows the blockdiagram of the fatigue tester (Fatiguron VFA-1kNA, A&D Orientec Co., Ltd, Saitama, Japan) that enables continuous measurements of nonlinear dynamic viscoelasticity and surface temperature during cyclic fatigue. Fatigue tests were carried out in a temperature range from 373 to 423 K under tension–tension stress-controlled loading and the frequencies of 10 and 20 Hz. The sinusoidal stress with the constant amplitude was imposed to the specimen. The minimum stress was 5.4 MPa and the maximum was in a range of 45–140 MPa. The data of the dynamic storage modulus, E', loss tangent, $\tan\delta$ and surface temperature rise, $\theta = T_S - T_0$, where T_S and T_0 were the surface temperature of the specimen and the ambient temperature, respectively, were continuously calculated and listed during cyclic fatigue. The surface temperature at the specimen center was continuously measured during cyclic fatigue with an infrared radiation thermometer producing a beam diameter of less than 2 mm long.

2.3. Nonlinear dynamic viscoelastic analysis

Since the imposed strain or stress must be large enough to ultimately lead to a fatigue failure, the deviation from the

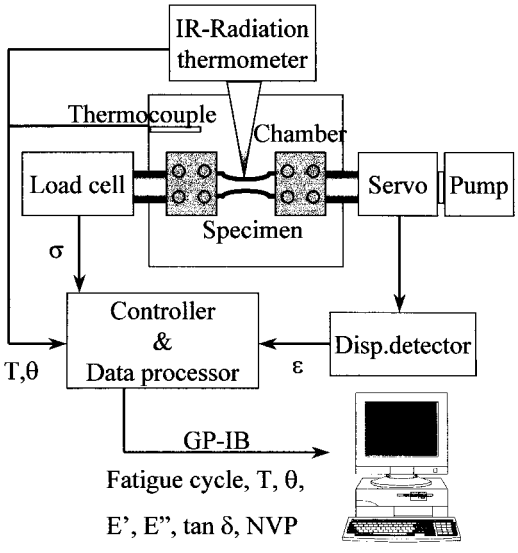

Fig. 2. Block diagram of fatigue tester that enables continuous measurement of nonlinear dynamic viscoelasticity and surface temperature during cyclic fatigue.

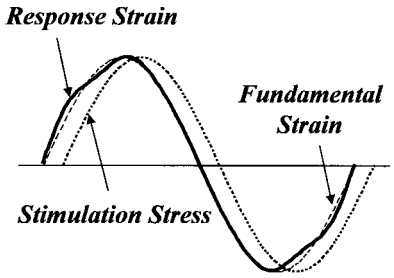

Fig. 3. Schematic representation of nonlinear response strain to sinusoidal stimulation stress with constant amplitude.

sinusoidal shape of the response strain signal to the sinusoidal stimulation stress was measured. Fig. 3 shows the schematic representation of nonlinear response strain to the sinusoidal stimulation stress with the constant amplitude. In the case of nonlinear viscoelastic behavior, when the sinusoidal stimulation stress, $\sigma(t)$ with angular frequency, ω is imposed to the specimen, the response strain, $\varepsilon(t)$ can be expanded by a Fourier series given by Eq. (1):

$$\varepsilon(t) = \varepsilon_1 \sin(\omega t + \delta_1) + \varepsilon_2 \sin(2\omega t + \delta_2) + \cdots + \varepsilon_n \sin(n\omega t + \delta_n) \quad (1)$$

where ε_1 and δ_1 are the fundamental strain amplitude and the phase difference angle, respectively. ε_2, $\varepsilon_3\cdots$, and $\delta_2, \delta_3\cdots$, are the higher harmonic strain amplitudes and the higher harmonic phase difference angles, respectively. The NVP [10], which corresponds to the degree of nonlinear viscoelasticity, is defined by Eq. (2).

$$\mathrm{NVP} = (\varepsilon_2 + \varepsilon_3 + \cdots \varepsilon_n)/\varepsilon_1 \quad (2)$$

where the number of higher harmonics, n was taken up to 10 in our study because the magnitude of ε_n for $n > 11$ is generally negligible.

2.4. Cross-section morphology

The microfailure state during the fatigue process was observed under an optical microscope (Optiphoto 200-D, Nikon Co., Ltd). The specimen for the optical microscopic observation was obtained by cutting off the test pieces, which were subjected to the cyclic fatigue for a certain fatigue cycle, N_{stop}. The cross-section of the specimen was precisely polished by metallurgical polishing technique with a buff and alumina powder and then was treated by ion etching. The cross-section morphology was observed in the central part and the longitudinal direction of the specimen. Also, the fracture surface after fatigue failure was observed on the basis of scanning electron microscopy (S-2120, Hitachi Co., Ltd). The fracture surface of the specimen was coated with gold for SEM observation in order to eliminate a charge-up of the specimen.

3. Result and discussion

3.1. S–N curve characteristics

Fig. 4(a) shows the temperature dependence of the S–N curves for the short glass-fiber reinforced nylon66 at 20 Hz. The S–N curve at each temperature can be approximated with the general Eq. (3) [16,17]:

$$\sigma_{max} = -A \log N + B \quad (3)$$

where σ_{max} and N are the maximum stress and fatigue cycle, respectively. A and B are the slope which means the fatigue resistance sensitivity and the intercept which means the apparent tensile strength, respectively. The relationship of Eq. (3) could be mentioned even in the case of the different frequency conditions, such as 10 Hz. Fig. 4(b) shows the temperature dependence of the slope A and the intercept B for Fig. 4(a). Both the slope and the intercept decreased almost linearly with increasing temperature in a low-temperature region below the glass transition temperature

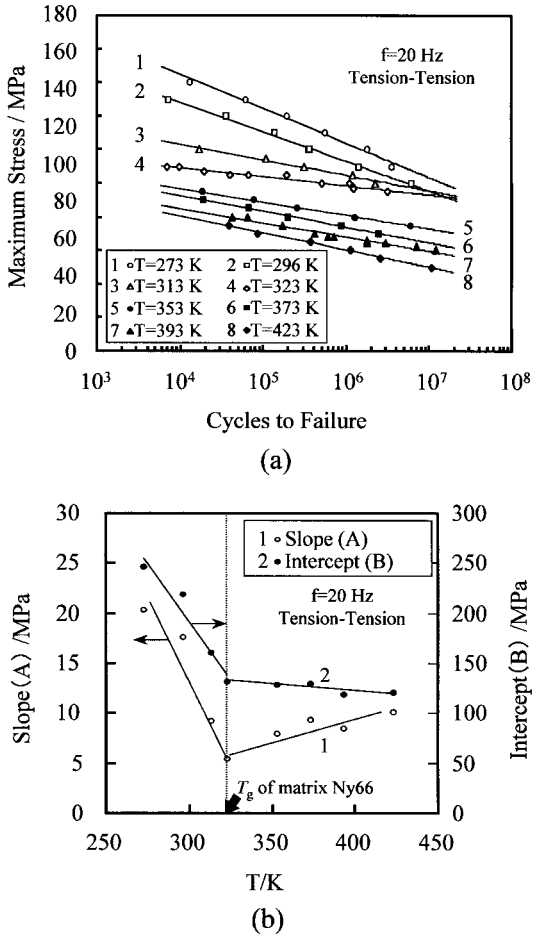

Fig. 4. (a) Temperature dependence of S–N curves for short glass-fiber reinforced nylon 66 at 20 Hz. (b) Temperature dependence of the slope A and intercept B of S–N curve at 20 Hz.

T_g of nylon 66 ($T \leqq T_g = 323$ K). On the other hand, in a high-temperature region above T_g ($T > T_g$), the slope A increased with increasing temperature, but the intercept B decreased slightly with increasing temperature. The temperature dependence of the magnitudes of A and B indicate that the fatigue characteristics can be expressed by two failure mechanisms depending on whether the testing temperature is below or above T_g. Therefore, the fatigue behavior and mechanism of the short glass-fiber reinforced nylon 66 during cyclic fatigue will be discussed next for the cases below and above T_g.

3.2. Fatigue behavior of short glass-fiber reinforced nylon 66 below T_g

3.2.1. Variation of nonlinear dynamic viscoelasticity during cyclic fatigue below T_g

Fig. 5 shows the variations of loss tangent, tan δ, surface temperature rise, θ and NVP with the number of fatigue cycle at 296 K as a function of maximum stress. Though the magnitude of tan δ increased slightly with an increase of maximum stress, the temperature dependence of tan δ did not show any noticeable change with fatigue cycle up to the fatigue failure and the magnitude of tan δ apparently increased just before the fatigue failure. The surface temperature increased with an increase of maximum stress at the same number of fatigue cycles. The surface temperature showed a remarkable increase in an initial short period of fatigue and also, in a final stage to a fatigue fracture in the stress-controlled fatigue test. When the magnitude of imposed stress was small, the surface temperature showed a little change over an intermediate fatigue process, indicating a quasi-thermal equilibrium state as shown in Fig. 5. In the case of large imposed stress, the surface temperature increased monotonically in the initial stage and the specimen fractured accompanying large plastic deformation due to a remarkable increase of specimen temperature. This is typical behavior for ductile failure. The magnitude of NVP as an index of nonlinear viscoelasticity increased and therefore, the fatigue lifetime decreased with an increase in the maximum stress. This apparently indicates that the fatigue behavior is closely related to the nonlinear viscoelastic characteristics. The change in NVP was observed in advance than the change of tan δ and the surface temperature. Therefore, it is reasonable to consider that the irreversible structural change being associated with nonlinear viscoelasticity did not appear in the final stage of fatigue fracture but was gradually stored in the specimen during cyclic fatigue.

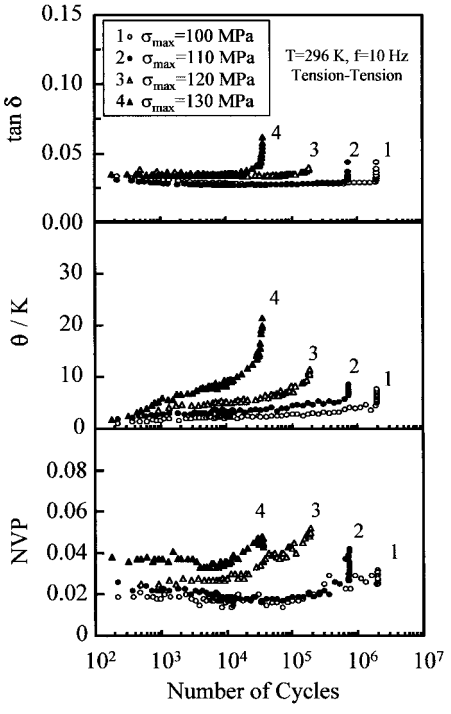

Fig. 5. Variations of tan δ, θ and NVP with the number of fatigue cycle at 296 K ($T < T_g$) as a function of maximum stress.

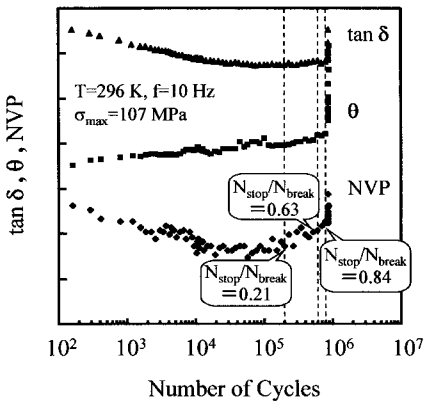

Fig. 6. Variations of tan δ, θ and NVP with the number of fatigue cycle under maximum stress of 107 MPa at 296 K ($T < T_g$).

3.2.2. Fracture mechanism during cyclic fatigue below T_g

Fig. 6 shows the variations of tan δ, θ and NVP with the number of fatigue cycle under the maximum stress of 107 MPa (fatigue cycles to failure of ca 9.5×10^5) at 296 K. The specimens were subjected to the number of cycles, N_{stop}, in order to observe the morphology of microfailure under optical microscope during cyclic fatigue.

The cross-section morphology of the specimen before cyclic stress loading is shown in Fig. 7. As shown in the optical microscope image, any defects were hardly observed in the composite specimen. When cyclic stress loading was applied to the specimen, a cluster of microcrack was observed in the matrix around the fiber ends as shown in Fig. 8(a). Fig. 8(a) shows the cross-section morphology of the specimen, which was obtained after being subjected to the cyclic fatigue of $N_{stop}/N_{break} = 0.21$ at 296 K. N_{stop} is the cycles that the fatigue test was interrupted for the morphorogical observation and N_{break} is the fatigue cycles to failure under the maximum stress of 107 MPa. Microvoids at the

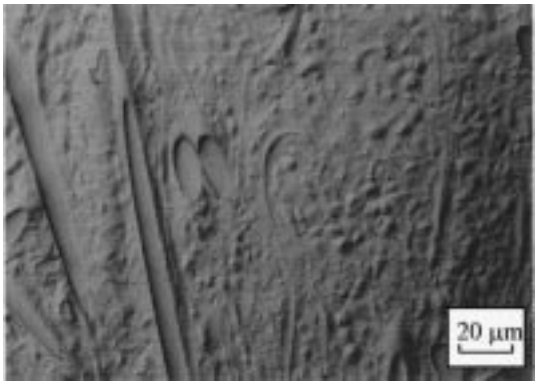

Fig. 7. Cross-section morphology of the specimen before cyclic stress loading.

interface of the fiber ends were formed as local defects. The magnitudes of tan δ, θ and NVP did not show any remarkable changes with the number of fatigue cycle until $N_{stop}/N_{break} = 0.21$. Also, Fig. 8(b) shows the cross-section morphology of the specimen, which was obtained after being subjected to the cyclic fatigue of $N_{stop}/N_{break} = 0.63$ at which the magnitudes of tan δ, θ and NVP gradually started to increase at 296 K. The initiation and connection of microcracks running from one fiber end to another one, corresponding to the formation of microcracks, was observed as shown in Fig. 8(b). It seems reasonable to consider that the interfacial failure was generated due to a shear stress concentration around the fiber ends. Fig. 8(c) shows the cross-section morphology of the specimen, which was obtained after being subjected to the cyclic fatigue of $N_{stop}/N_{break} = 0.84$ at 296 K. The magnitudes of tan δ, θ and NVP rapidly increased at $N_{stop}/N_{break} = 0.84$. The crack propagation connecting the interfacial failure at the fiber ends and also the fracture of glass fiber were observed.

The fatigue failure mechanism of the short glass-fiber reinforced nylon 66 below T_g is discussed on the basis of the results of Figs. 5–8. Fig. 9 shows a schematic representation of the fatigue failure process (stages 1–4) below T_g. The stage 1 is a void formation and an initiation of microcrack generally at glass-fiber ends of the highest stress concentration as shown in Fig. 8(a). The fiber ends were weakly bonded to the matrix because of no surface treatment of fiber ends. The stage 2 is a propagation of microcracks around the glass-fiber ends as shown in Fig. 8(b). The stage 3 is a crack growth among the fiber ends as shown in Fig. 8(c). The final stage 4 is a fast crack growth in a brittle manner generally perpendicular to the stress loading direction resulting in the final failure of the specimen. The magnitude of NVP gradually increased at the intermediate stage of cyclic fatigue of $N_{stop}/N_{break} = 0.63$ under the maximum stress of 107 MPa at 296 K as shown in Fig. 6. The increase in NVP during the fatigue process

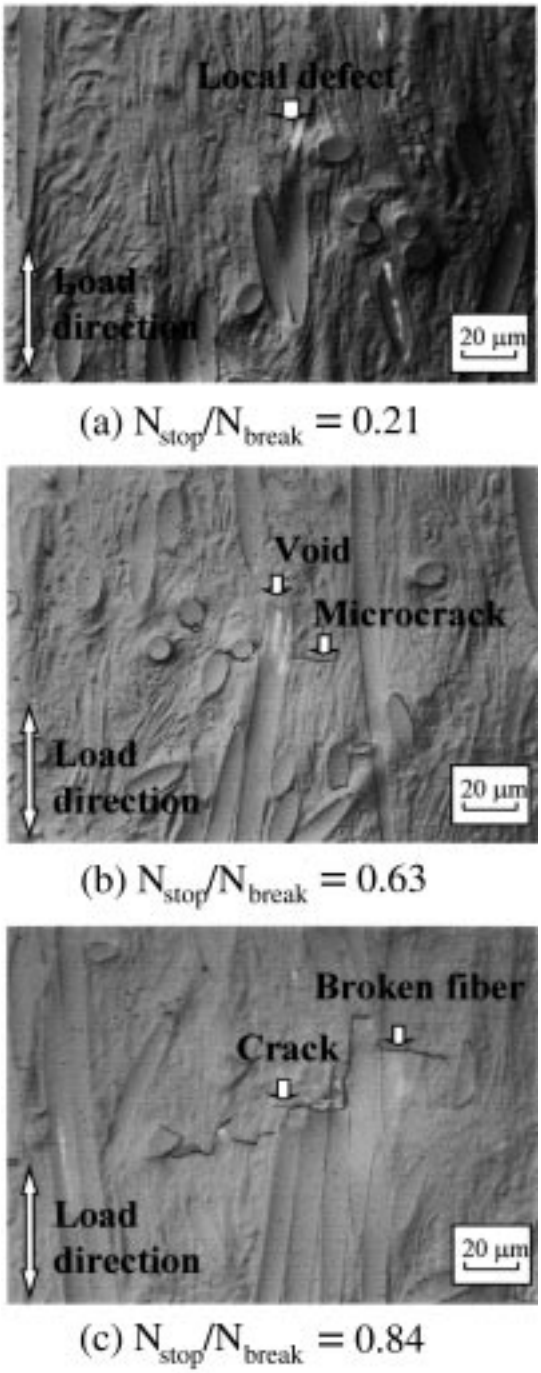

Fig. 8. Cross-section morphology of the specimen, which was obtained to be subjected to the cyclic fatigue of: (a) $N_{stop}/N_{break} = 0.21$; (b) $N_{stop}/N_{break} = 0.63$ and (c) $N_{stop}/N_{break} = 0.84$ at 296 K.

remarkably related to the propagation of microcracks and the crack growth corresponding to the stage 2. Since the fatigue behavior was closely related to the nonlinear viscoelasticity as discussed above, the modeling of fatigue mechanism and the prediction of lifetime might be possible on the basis of nonlinear dynamic viscoelasticity measurements [10].

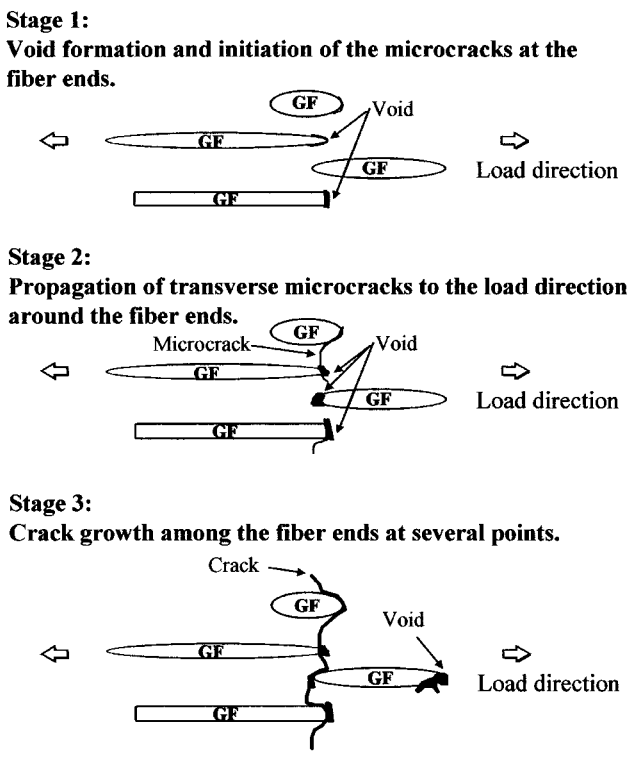

Fig. 9. Schematic representation of fatigue failure process below T_g.

3.3. Fatigue behavior of short glass-fiber reinforced nylon 66 above T_g

3.3.1. Variation of nonlinear dynamic viscoelasticity during cyclic fatigue above T_g

Fig. 10 shows the variations of loss tangent, tan δ, surface temperature rise, θ and NVP, with the number of fatigue cycle at 393 K as a function of the maximum stress. The magnitude of tan δ increased with an increase of maximum stress. The magnitude of tan δ decreased with an increase of the number of fatigue cycle, and showed the minimum just before the fatigue failure. This behavior indicates a considerable increase in the contribution of elastic term, such as an orientation of molecular chains under cyclic loading. The surface temperature shows little change with increasing maximum stress. The surface temperature almost remained constant in the intermediate fatigue process after θ reached a quasi-thermal equilibrium state and slightly rose in the final stage of fatigue test. Also, the magnitude of NVP increased with an increase in maximum stress. The magnitude of NVP remarkably increased just before the fatigue failure and this behavior was observed in advance than the steep increases of tan δ and the surface temperature. Thus, Fig. 10 apparently indicates that the irreversible structural change during the cyclic fatigue test of the composite

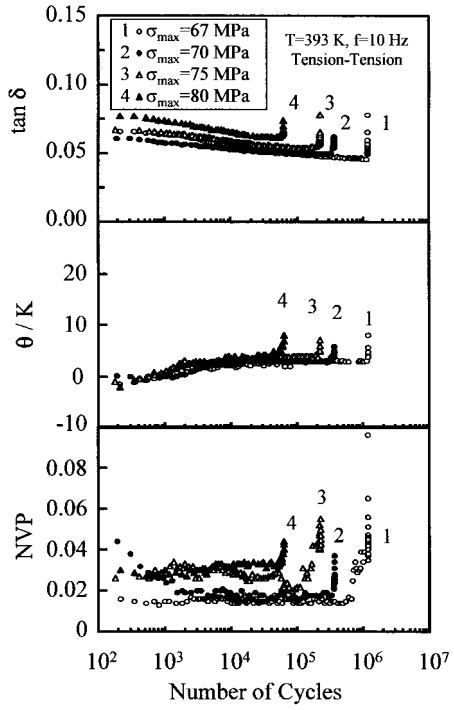

Fig. 10. Variations of tan δ, θ and NVP with the number of fatigue cycle at 393 K ($T > T_g$) as a function of maximum stress.

above T_g strongly related to the nonlinear viscoelastic characteristics.

3.3.2. Fracture mechanism during cyclic fatigue above T_g

Fig. 11 shows the variations of tan δ, θ and NVP with the number of fatigue cycle under the maximum stress of 67 MPa (fatigue cycles to failure of ca. 9.2×10^5) at 393 K. The specimen has been subjected to the cyclic fatigue for the prescribed fatigue cycle, in order to observe the morphology of microfailure under optical microscope during the fatigue process.

Fig. 12(a) shows the cross-section morphology of the specimen which was obtained after being subjected to the cyclic fatigue of $N_{stop}/N_{break} = 0.02$ at 393 K. Little

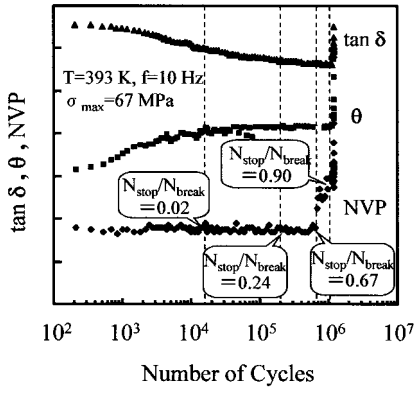

Fig. 11. Variations of tan δ, θ and NVP with the number of fatigue cycle under maximum stress of 67 MPa at 393 K ($T > T_g$).

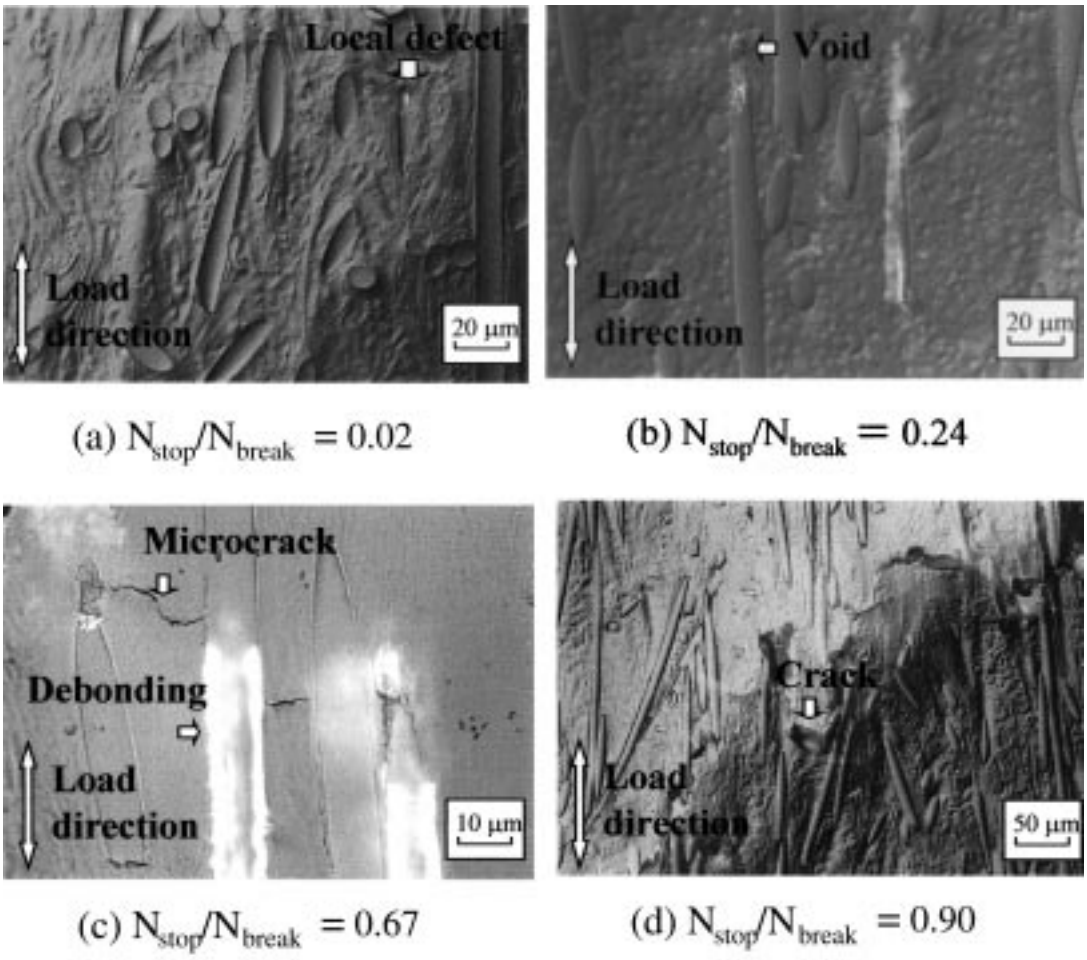

Fig. 12. Cross-section morphology of the specimen, which was obtained to be subjected to the cyclic fatigue of: (a) $N_{stop}/N_{break} = 0.02$, (b) $N_{stop}/N_{break} = 0.24$, (c) $N_{stop}/N_{break} = 0.67$ and (d) $N_{stop}/N_{break} = 0.90$ at 393 K.

microvoids or local defects were observed at the fiber ends that were weakly bonded to the matrix. However, the magnitude of NVP did not show any change up to $N_{stop}/N_{break} = 0.02$ and the surface temperature reached to a quasi-thermal equilibrium state. Fig. 12(b) shows the cross-section morphology of the specimen, which was obtained after being subjected to the cyclic fatigue of $N_{stop}/N_{break} = 0.24$ at 393 K. The magnitude of NVP did not change up to $N_{stop}/N_{break} = 0.24$. The microvoids were formed at the interface of the fiber ends as the initiator of microfailure since the local stress intensity was high at the fiber ends. Fig. 12(c) shows the cross-section morphology of the specimen, which was obtained after being subjected to the cyclic fatigue of $N_{stop}/N_{break} = 0.67$ at 393 K. The magnitude of NVP gradually increased at $N_{stop}/N_{break} = 0.67$. The microfailure propagated at the almost interfacial region between matrix nylon 66 and glass-fiber surface. Debonding might take place in a shear mode at the fiber ends, where the shear stress was the highest. The deformation and fracture of the matrix between fibers, pull-out fibers were observed and then the crack walls were formed by debonding along the fiber sides as shown in Fig. 12(c). Fig. 12(d) shows the cross-section morphology of the specimen, which was obtained after being subjected to the cyclic fatigue of $N_{stop}/N_{break} = 0.90$ at 393 K. The magnitude of NVP remarkably increased at $N_{stop}/N_{break} = 0.90$. The crack walls remained being connected by bridging at several points. The crack propagated in a ductile manner and finally the matrix was led to the final failure when the crack grew up to the critical size.

Fig. 13 shows the schematic representation of the fatigue process of the composites above T_g based on the results of Figs. 10–12. The stage 1 corresponds to the local defect formation due to cyclic deformation at the locations of highest stress intensity such as at the fiber ends as shown in Fig. 12(b). The damage accumulated, resulting in the void formation, mainly at the fiber ends. The stage 2 is the propagation of the interfacial microfailure due to debonding along the fiber sides and the deformation of matrix resin between fibers as shown in Fig. 12(c). The stage 3 shows the crack walls connected by bridging them and the crack growth between fibers as shown in Fig. 12(d). The final stage 4

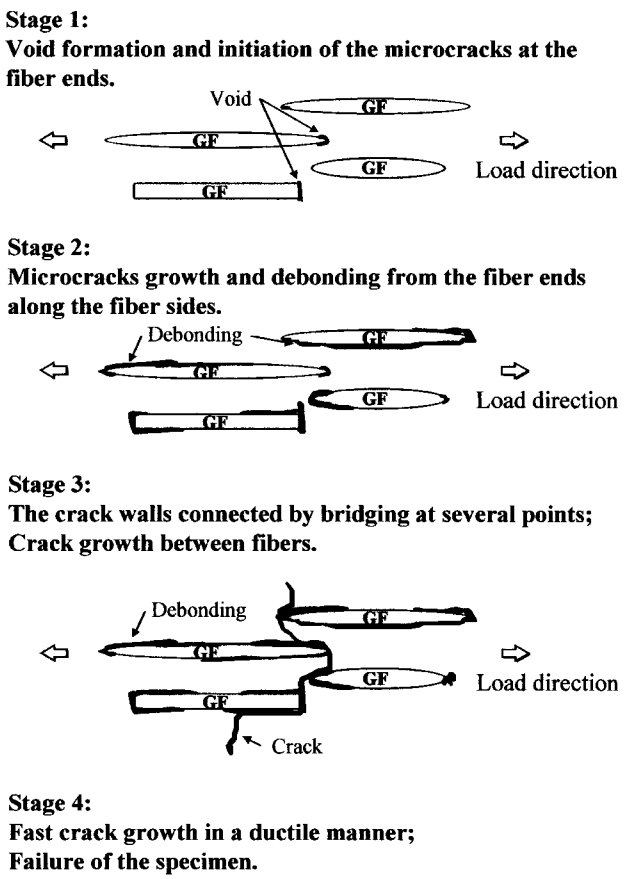

Fig. 13. Schematic representation of fatigue failure process above T_g.

shows that the specimen finally failed after the fast crack growth in a ductile manner. The magnitude of NVP remarkably increased in the intermediate stage of cyclic fatigue up to $N_{stop}/N_{break} = 0.67$ under the maximum stress of 67 MPa at 393 K as mentioned in Fig. 11. This behavior showed the same tendency without depending on the temperature. Therefore, it is apparent that the irreversible structural changes, such as debonding and microcrack growth, strongly related to nonlinear viscoelasticity without depending on the measuring temperature below or above T_g. However, the final fatigue failure took place in a brittle and in a ductile manner below and above T_g, respectively.

3.4. Fatigue fracture surface below T_g and above T_g

Fig. 14 shows SEM images of the fatigue fracture surface (a) below T_g and (b) above T_g. In the case of the fatigue failure below T_g as shown in Fig. 14(a), the glass-fibers were broken into fairly short pieces and then the number of pull-out fibers was not large. On the other hand, many pull-out fibers were observed on the fracture surface in the case of the fatigue failure above T_g as shown in Fig. 14(b). These results correspond to the two different fatigue mechanisms based on the different degree of matrix ductility, depending on the testing temperature below or above T_g.

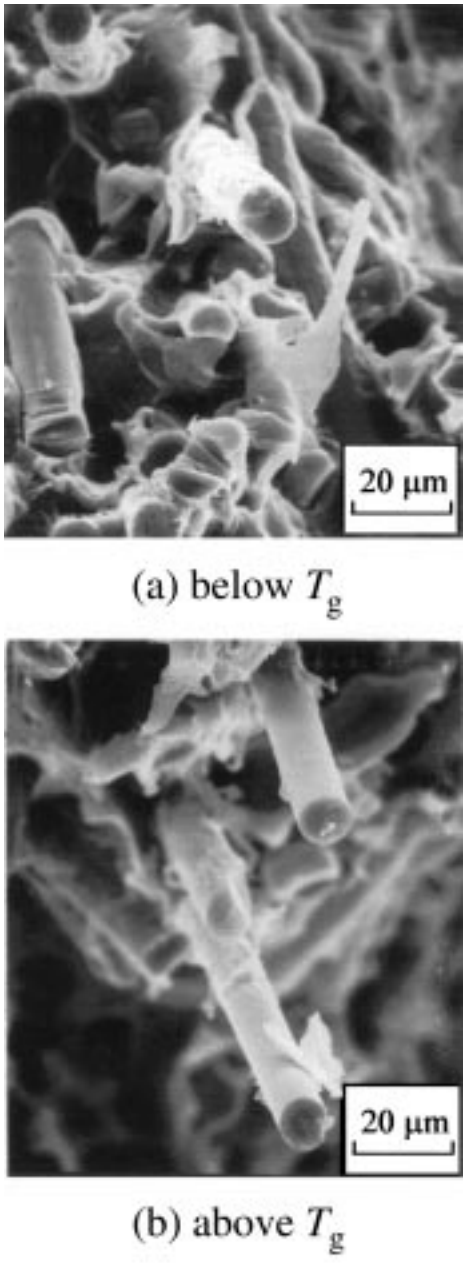

Fig. 14. SEM images of fatigue fracture surface: (a) below T_g and (b) above T_g.

4. Conclusions

The fatigue mechanism of short glass-fiber reinforced nylon 66 under stress control fatigue tests was studied on the basis of the nonlinear dynamic viscoelasticity measurements. Microvoid formation at the fiber ends due to the stress concentration was found to be essential origin of fatigue failure of the composites, without depending on the measuring temperature. When the magnitude of NVP as an index of nonlinear viscoelasticity remarkably increased in the intermediate stage of cyclic fatigue, the debonding occurred and microcrack grew. Therefore, it can be concluded that the irreversible structural changes such as

debonding and microcrack growth remarkably related to the nonlinear viscoelasticity. The fatigue characteristics can be classified by the two failure mechanism depending on whether the testing temperature is below or above T_g. In the case of the fatigue mechanism below T_g, the microcracks propagated around the fiber ends, and then the cracks dominantly propagated between the fiber ends in a brittle manner. While, in the case of the fatigue mechanism above T_g, the microcracks propagated accompanied debonding along the fiber sides and forming the crack walls, and then the crack walls dominantly remained being connected by bridging in a ductile manner. The fatigue behavior and failure mechanism obtained in this study is considered to be essential for other types of short glass-fiber reinforced composites.

References

[1] Lang RW, Manson JA, Hertzberg RW. J Mater Sci 1987;22:4015.
[2] Hertzberg RW, Manson JA. Fatigue of engineering plastics. New York: Academic Press, 1980.
[3] Karger-Kocsis J, Friedrich K. Composites 1988;19:105.
[4] Sato N, Kurauchi T, Sato S, Kamigaito O. J Mater Sci 1991;26:3891.
[5] Horst JJ, Spoormaker JL. Polym Engng Sci 1996;36:2718.
[6] Takahara A, Yamada K, Kajiyama T, Takayanagi M. J Appl Polym Sci 1980;25:597.
[7] Takahara A, Yamada K, Kajiyama T, Takayanagi M. J Appl Polym Sci 1981;26:1085.
[8] Takahara A, Magome T, Kajiyama T. J Polym Sci, Polym Phys Ed 1994;32:839.
[9] Yamashita A, Takahara A, Kajiyama T. Compos Interfaces 1999;6:247.
[10] Jo NJ, Takahara A, Kajiyama T. Polym J 1993;25:721.
[11] Jo NJ, Takahara A, Kajiyama T. Polym J 1994;26:1024.
[12] Liang T, Tokunaga K, Yamashita A, Takahara A, Kajiyama T. Polym Bull 1996);36:477.
[13] Jo NJ, Takahara A, Kajiyama T. Polymer 1997;38:5195.
[14] Liang T, Takahara A, Saito K, Kajiyama T. Polym J 1996;28:801.
[15] Liang T, Takahara A, Saito K, Kajiyama T. Polymer 1998;22:5387.
[16] Zilvar V. J Macromol Sci, Phys 1971;B5:271.
[17] Handa K, Kato A, Narisawa I. J Appl Polym Sci 1999;72:1783.